THE
EMBO
JOURNAL

Structural diversity of bacterial flagellar motors

Songye Chen[1,6], Morgan Beeby[1,2,6],
Gavin E Murphy[1,7], Jared R Leadbetter[3],
David R Hendrixson[4], Ariane Briegel[1,2],
Zhuo Li[1,2,8], Jian Shi[1,2], Elitza I Tocheva[1],
Axel Müller[5], Megan J Dobro[1]
and Grant J Jensen[1,2,*]

[1]Division of Biology, California Institute of Technology, Pasadena, CA, USA, [2]Howard Hughes Medical Institute, California Institute of Technology, Pasadena, CA, USA, [3]Division of Environmental Science and Engineering, California Institute of Technology, Pasadena, CA, USA, [4]Department of Microbiology, University of Texas Southwestern Medical Center, Dallas, TX, USA and [5]Division of Chemistry, California Institute of Technology, Pasadena, CA, USA

The bacterial flagellum is one of nature's most amazing and well-studied nanomachines. Its cell-wall-anchored motor uses chemical energy to rotate a microns-long filament and propel the bacterium towards nutrients and away from toxins. While much is known about flagellar motors from certain model organisms, their diversity across the bacterial kingdom is less well characterized, allowing the occasional misrepresentation of the motor as an invariant, ideal machine. Here, we present an electron cryotomographical survey of flagellar motor architectures throughout the Bacteria. While a conserved structural core was observed in all 11 bacteria imaged, surprisingly novel and divergent structures as well as different symmetries were observed surrounding the core. Correlating the motor structures with the presence and absence of particular motor genes in each organism suggested the locations of five proteins involved in the export apparatus including FliI, whose position below the C-ring was confirmed by imaging a deletion strain. The combination of conserved and specially-adapted structures seen here sheds light on how this complex protein nanomachine has evolved to meet the needs of different species.

*Corresponding author. Division of Biology, California Institute of Technology, 1200 E. California Blvd, MC114-96, Pasadena, CA 91125, USA. Tel.: +1 626 395 8827; Fax: +1 626 395 5730;
E-mail: Jensen@caltech.edu
[6]These authors contributed equally to this work
[7]Present address: Laboratory of Cell Biology, Center for Cancer Research, National Cancer Institute, National Institutes of Health, Bethesda, MD 20892, USA
[8]Present address: Molecular and Cellular Biology Department, City of Hope Beckman Research Institute, Electron Microscopy Facility, Duarte, CA 91010, USA

Introduction

The bacterial flagellum is a paradigm in modern molecular biology. Its structural complexity, multi-phasic and strictly regulated self-assembly, mechanical capabilities, functional interdependence with the chemosensory system, and both pathogenic and ecophysiological importance have made it central to studies and discussions in both the scientific and popular literature (Berg, 2003; McCarter, 2006; Pallen and Matzke, 2006; Chevance and Hughes, 2008; Minamino *et al*, 2008; Sowa and Berry, 2008; Snyder *et al*, 2009). The flagellum consists of a motor also known as the basal body, a flexible linker termed the hook, and a filament that behaves as a helical propeller and is typically many times the length of the bacterium itself. The motor converts ion flux across the cytoplasmic membrane into a torque that rotates the flagellum. In some organisms such as *Escherichia coli*, counterclockwise rotation generates thrust that propels the cell forward. Signals from chemoreceptor arrays (Briegel *et al*, 2009) modulate the probability of the flagellar motor reversing direction (to spin clockwise) (Hazelbauer *et al*, 2008), which causes the bacterium to randomly re-orient. Thus, if a bacterium detects that it is swimming towards nutrients, the chemosensory system can prolong its movement in a specific direction.

Although all bacterial flagella share similarities in structure and mechanism, extensive variation in number, placement and usage exist between species. While cells such as *Vibrio cholerae* and *Caulobacter crescentus*, for example, exhibit a single polar flagellum, others, including *Salmonella enterica* and *E. coli* distribute several or many flagella around their periphery. Under different conditions, some bacteria alternate between polar and lateral flagellar systems (McCarter, 2004). The flagella of spirochaetes do not typically pierce the outer membrane, but instead remain in the periplasm where they rotate and/or contort the cell (Murphy *et al*, 2006; Liu *et al*, 2009; Kudryashev *et al*, 2010). Flagellar rotation is powered either by a proton-motive force (e.g., *E. coli*) or by a sodium-motive force (e.g., *V. cholerae*). The 'run and tumble' swimming mode that switches between clockwise and counter-clockwise rotations is best known, but other bacteria function differently, for example by varying the speed of a unidirectional motor. The molecular architectures of the helical flagellar filaments are also diverse (Galkin *et al*, 2008).

The flagellar motor is constructed from >20 proteins, and its basic morphology consists of an extended axial rod with coaxial rings termed the L-, P-, S-, M- and C-rings based on their locations relative to the cell. Previous analyses of flagellar motor genes have shown that they are widely distributed throughout and conserved across many bacterial lines of descent, but it has not been clear how observed sequence variations relate to the final structure of the macromolecular complex (Pallen *et al*, 2005; Liu and Ochman, 2007; Snyder *et al*, 2009). Structural studies of the motor to date have focussed on a small number of key organisms and have been hampered by the motor's size, complexity,

membrane localization and attachment to the cell envelope. These factors make motors difficult if not impossible to purify intact. X-ray crystallography has nevertheless revealed the structures of some of the isolated motor proteins, and complementary biochemical and genetic analyses have located many of them within the intact motor. Single-particle cryoEM studies have produced nanometre-resolution structures of the purified *S. enterica* motor, albeit without stators or the export apparatus (Thomas *et al*, 2006). In just the past few years, the development of electron cryotomography (ECT) has made it possible to image the structures of complete motors within intact cells in 3D to 'macromolecular' (several nanometres) resolution (Li and Jensen, 2009; Milne and Subramaniam, 2009). The first *in situ* structures have been from the thin spirochaetes *Treponema primitia* (Murphy *et al*, 2006) and *Borrelia burgdorferi* (Liu *et al*, 2009; Kudryashev *et al*, 2010). Those species demonstrated large peripheral structures not seen in the *S. enterica* single-particle reconstruction, hinting that the diversity of motor structures might be great.

Results and discussion

Data collected and overall appearance of the motors

We sought to sample the structural diversity of bacterial flagellar motors. To this end, we imaged the flagellar motors from 11 phylogenetically diverse bacteria chosen for their general interest as model organisms; involvement in animal host associations or free-living lifestyles, and suitability for ECT. The selected bacteria include those with polar (*C. crescentus* and *Campylobacter jejuni*), peritrichous (*S. enterica* and *E. coli*) and periplasmic (the spirochaetes *T. primitia* and *B. burgdorferi*) flagella. Bacteria employing Na-driven motors (*V. cholerae*) or 'sheathed' flagella (*V. cholerae* and *Helicobacter hepaticus*) were also included (see Supplementary Table S1 for comprehensive details on the phylogenetics and characteristics of each motor). Using high-throughput imaging methods (Suloway *et al*, 2009), for each species hundreds of cryotomograms of whole cells were collected. Subtomograms containing motors were computationally extracted from the data, mutually aligned, averaged and cylindrically symmetrized to obtain resolutions of a few nanometres (see Materials and methods).

While all the motors had clear similarities, their overall appearances were strikingly diverse (Figure 1). Comparison of the *S. enterica* structure with a previous single-particle cryoEM reconstruction (Thomas *et al*, 2006) exhibited similar features at similar positions along the rod and C-ring (Figure 2, left panel), cross-validating the two approaches, but the ECT reconstruction here also showed the position and curvature of the membranes and elements of the export apparatus, albeit at lower resolution. To highlight similarities among the motors, we generated a 'generic' motor by aligning and averaging the axial slices of all 11 structures. As shown in Figure 2 (right panel), the core structure of the rod, L-, P-, S-, M- and C-rings, and the export apparatus, as well as their relative locations with regard to the membranes are consistent across all motors. Because the C-rings of different species have different diameters, several C-rings appear in the generic average. This is in contrast with the other parts such as the rod, the LP- and MS-ring complexes and the export apparatus, whose boundaries remain sharp,

indicating high structural conservation in their structures across species. Using these conserved features as landmarks, the densities present in the 11 independent motor reconstructions were carefully compared with those in the generic and *S. enterica* structures and assigned to known structures where possible (Figure 3). To assist in this process and provide insight into the differences, we correlated our imaging results with genomic data for each organism, sequencing and annotating new genomes when necessary. Lists of orthologues of known flagellar proteins were hand-curated (see Supplementary Table S2) and novel, previously unrecognized flagellar motor gene products were sought using their co-occurrence with motor genes in operons.

Export apparatus

The MS-ring in the inner membrane serves as the starting point for motor assembly. As expected, homologues of the sole component protein of the MS-ring, FliF, are present in all genomes. The periplasmic S-ring is correspondingly clear in all the organisms, but the membrane-embedded M-ring is less distinct due to contrast matching with the membrane. Compared with the single-particle reconstruction of *S. enterica*, there are three major additional densities present in the ECT reconstructions below the MS-ring: a convex dome bulging into the cytoplasm immediately beneath the MS-ring, a torus 10 nm lower and a spherical density 10 nm below the torus (Figure 4, schematic). Based on their position, presence in the intact cells, and absence in the single-particle reconstruction, we hypothesized that these three additional densities correspond to the dedicated type III secretion system (T3SS) that exports the proteins that form the rod, hook and filament through the hollow inner bore of the assembling flagellum. This flagellar export apparatus typically consists of six transmembrane (FlhA, FlhB, FliO, FliP, FliQ and FliR) and three soluble (FliH, FliI and FliJ) proteins.

The transmembrane proteins must reside at least in part in the dome, as it appears to be the continuation of the cytoplasmic membrane across the motor. The bulging of the dome (most prominent in *E. coli*, *C. jejuni*, *B. burgdorferi*, *T. primitia* and *Acetonema longum*) may be necessary to accommodate the transmembrane proteins, as the circular area within the plane of the M-ring in single-particle reconstructions was judged insufficient (Suzuki *et al*, 2004). Both FlhA and FlhB possess C-terminal cytoplasmic domains at the end of long (~30 amino acid) linkers (Saijo-Hamano *et al*, 2004, 2010; Zarivach *et al*, 2008; Moore and Jia, 2010; Worrall *et al*, 2010). The torus immediately below the dome, therefore, likely corresponds to their cytoplasmic domains, and the weak density seen between the dome and the torus in some of the reconstructions (most notably *S. enterica*) to the linkers. Together, the cytoplasmic domains of FlhA and FlhB have been referred to as the 'export platform', and may have been at least in part what was previously referred to as the 'C rod' in freeze-etch images (Katayama *et al*, 1996). Structures of homologues of these domains are available (Zarivach *et al*, 2008; Saijo-Hamano *et al*, 2010), and match the dimension of the torus reasonably well, though it remains unclear how they pack together or how many are required to complete the ring.

We reasoned that the spherical density below the torus likely corresponded to the ubiquitous ATPase FliI. FliI is thought to oligomerize into a roughly spherical cyclic
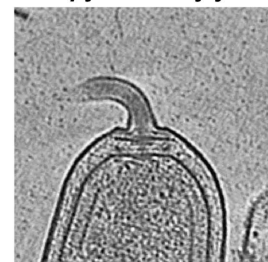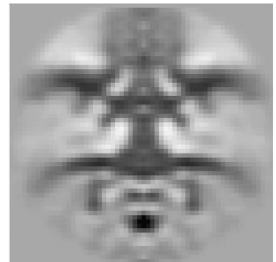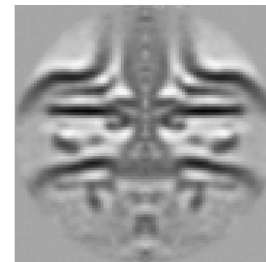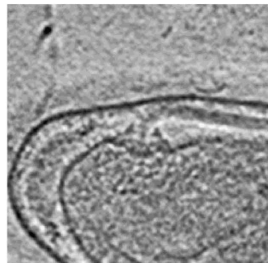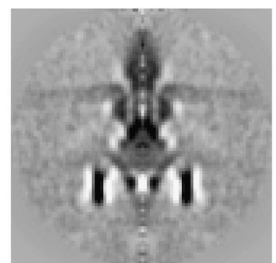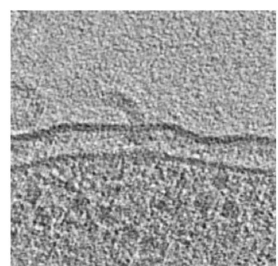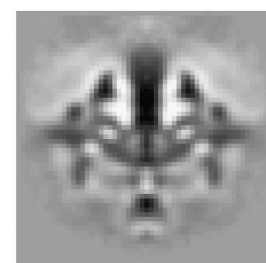
Hylemonella gracilis
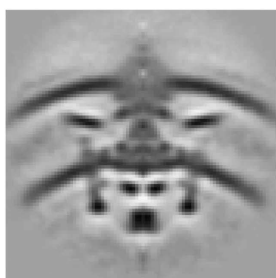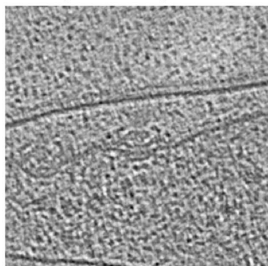

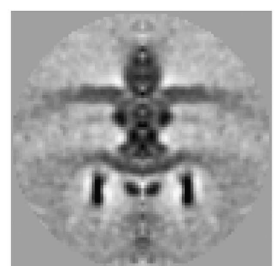*Campylobacter jejuni*

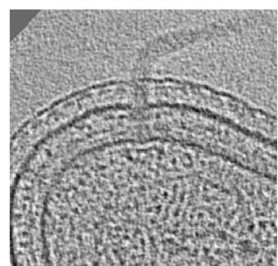*Vibrio cholerae*

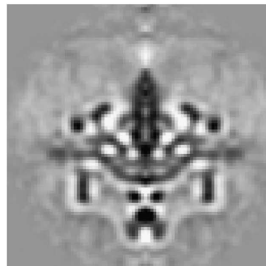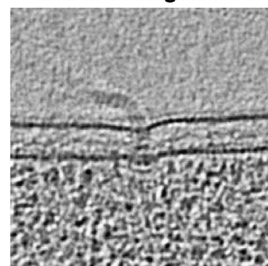*Helicobacter hepaticus*

Salmonella enterica

Treponema primitia
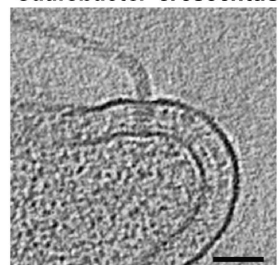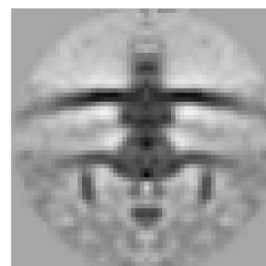

Escherichia coli

Borrelia burgdorferi

Caulobacter crescentus

Acetonema longum

Hyphomonas neptunium
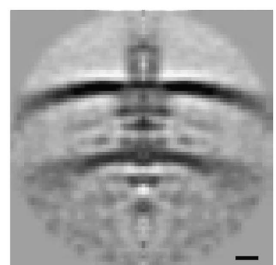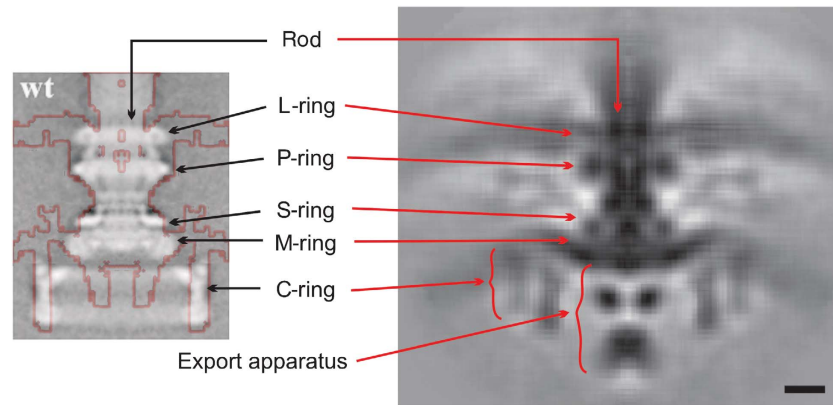
Figure 2 Structure of the common core and its comparison with an earlier cryoEM single-particle reconstruction. Left: Isosurface of the *S. enterica* motor obtained by ECT and subtomogram averaging (red line) superimposed on an earlier single-particle reconstruction of purified basal bodies from the same organism (grey levels) (Thomas *et al*, 2006). Right: A generic motor structure obtained by aligning and averaging the axial slices of all 11 motors reconstructed here. Scale bar, 10 nm.
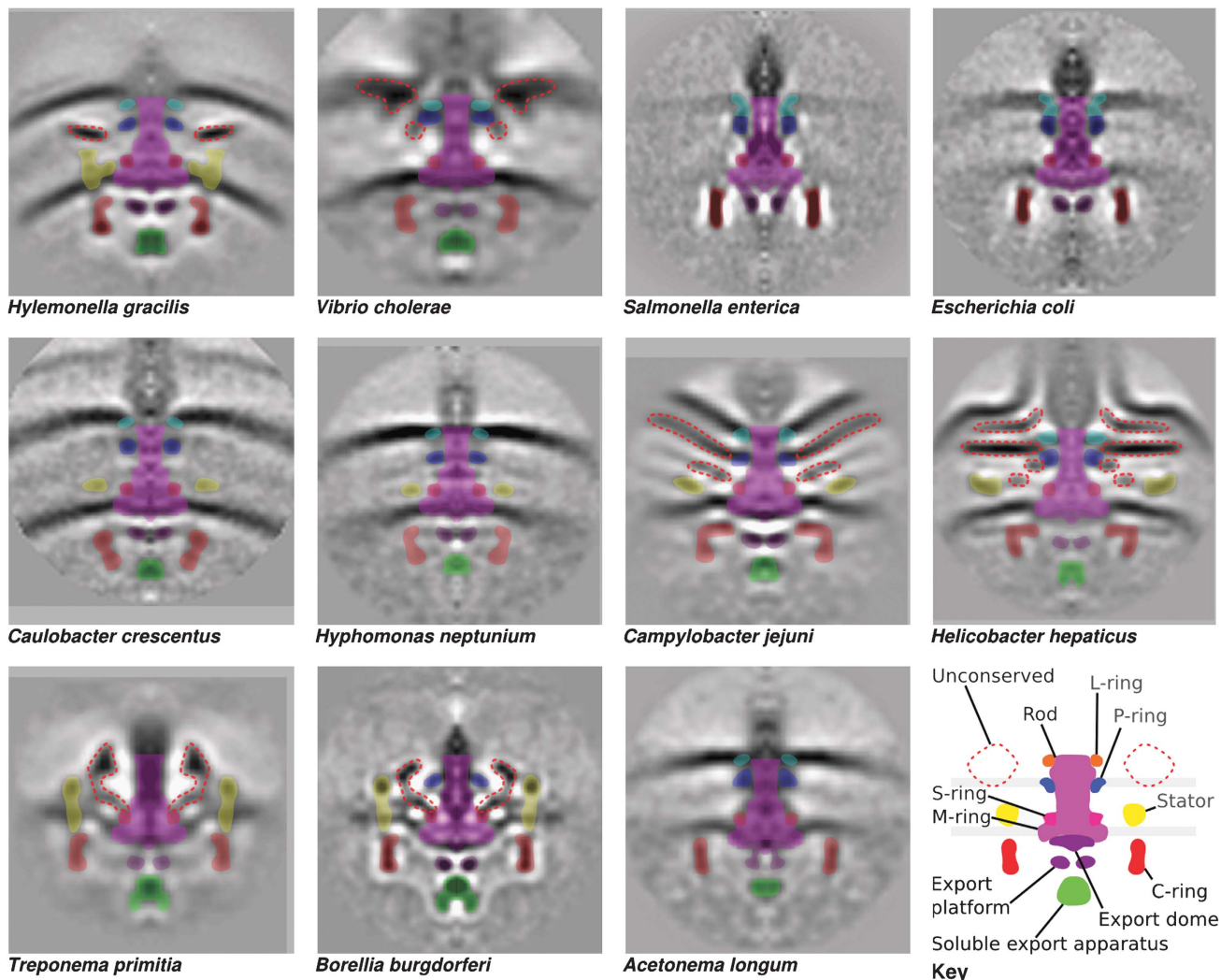
Figure 3 Assignment of densities. Manual segmentation of conserved (solid colours) and unconserved (dotted lines) motor components based on visual inspection. The conserved components from bottom to top are soluble export apparatus (FliH, FliI and FliJ); export platform and dome (FlhA, FlhB, FliO, FliP, FliQ and FliR); C-ring (FliG, FliM and FliN); MS-ring (FliF); stators (MotA and MotB in the H^+-dependent stators or PomA and PomB in the Na^+-dependent stators); rod (FliE, FlgB, FlgC, FlgF and FlgG); P-ring (FlgI); and L-ring (FlgH).

Figure 1 Flagellar motor structures obtained by ECT and subtomogram averaging. Left column: 20-nm thick central slices through tomograms of individual cells exhibiting flagellar motors, arranged in the same order as they appear on the phylogenetic tree shown in Supplementary Figure S2. Scale bar, 50 nm. Right column: Axial slices through average reconstructions of each motor. Scale bar, 10 nm. (Note that the motor structure of *T. primitia* was published previously; Murphy *et al*, 2006.)
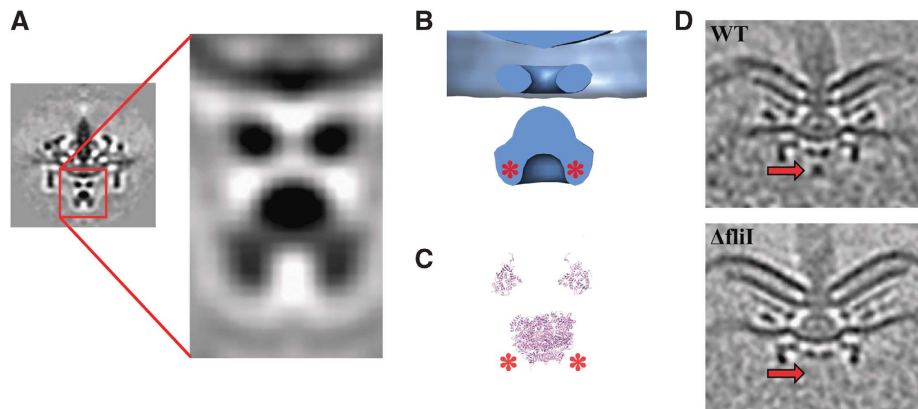
Figure 4 Structure of the export apparatus. (**A**) Enlarged view of the *B. burgdorferi* export apparatus and (**B**) 3D isosurface illustrating from top to bottom the export dome, torus and spherical density. (**C**) Atomic models of the cytoplasmic domains of FlhA above and the hexameric F1-ATPase, a homologue of FliI, shown at the same scale as (**B**) to show the correspondence of their sizes to the torus and spherical density. (**D**) Wild-type (top) and *ΔfliI* (bottom) *C. jejuni* motors confirming that the spherical density (red arrows, present above and absent below) is FliI.

hexamer ∼9.5 nm in diameter (Claret *et al*, 2003), as illustrated by models based on the homologous F1-ATPase (Miwa and Yoshida, 1989) using crystal structures of FliI (Imada *et al*, 2007) or the FliI homologue EscN from the T3SS (Zarivach *et al*, 2007). This is in good agreement with the ∼10 nm diameter seen for the spherical density in the reconstructions presented here (Imada *et al*, 2007; Zarivach *et al*, 2007). To test the hypothesis that this spherical density corresponds to FliI, we recorded cryotomograms of a *C. jejuni* strain lacking the *fliI* gene. *C. jejuni* was chosen for this test because it can be manipulated genetically and exhibits a clear density in this region. Despite the absence of *fliI*, the deletion strain produced sufficient motors for subtomogram averaging, consistent with a recent study in *Salmonella* (Paul *et al*, 2008), demonstrating that assembly can proceed without an absolute requirement for the export apparatus component FliI. The structure of the *fliI*-deletion strain was essentially identical to the wild type except for the spherical density, which was completely absent, confirming its identity (Figure 4D).

In addition to FliI, two other proteins (FliH and FliJ) are also probably part of the spherical density. FliH, a FliI regulator encoded in the genomes of all organisms but *Hyphomonas neptunium*, is known to bind FliI at its extreme N-terminus. If the FliI hexamer is oriented towards the membrane in the same way as its homologue, the F1-ATPase, as suggested in a recent study (Ibuki *et al*, 2011), the N-terminus of each FliI monomer will point towards the cytoplasm. The cytoplasmic-facing protuberances on the spherical density are, therefore, likely FliH (asterisks in Figure 4B). The poorly conserved FliJ has been shown to occupy the central pore of the FliI hexamer, and is structurally similar to the γ-subunit of the F1F0-ATPase (Ibuki *et al*, 2011). Although *fliJ* could not be detected in some organisms, its absence may be due to a difficulty in identifying the poorly conserved sequence.

The assignment of the torus as the cytoplasmic domains of FlhA and FlhB and the spherical density as the FliHIJ complex rationalize why in a recent tomographic study of detergent-treated *B. burgdorferi* cells, the torus but not the spherical density was visible (because the torus is covalently linked to the dome) (Liu *et al*, 2009). These assignments also

explain why the spherical density is faint in the reconstructions of *S. enterica* and *E. coli* presented here: *S. enterica* and *E. coli* were included in the present survey because they are key model systems, but because both of them are too thick for high resolution ECT, these cells were gently lysed just before freezing (see Materials and methods), which would likely disrupt the localization of soluble proteins like FliI. The shape and prominence of the FliHIJ density in the average reconstructions may also be affected by the facts that FliI occurs as both a monomer and a hexamer and is also known to interact with the relatively distant C-ring, and may not therefore occupy a consistent location.

C-ring

Assembling around FliF (the MS-ring) and the export apparatus is the C-ring, which is involved in export, torque generation and directional switching. Accordingly, the C-ring is present in all 11 organisms and three C-ring structural genes, *fliG*, *fliM* and *fliN*, are conserved across all genomes. Considerable variation is evident, however, in the appearance and diameter of the C-rings, which range from 34 nm in *C. crescentus* to 57 nm in *T. primitia* (Figures 1 and 3). Consistent with the cryoEM single-particle reconstruction of the *S. enterica* motor (Thomas *et al*, 2006), all the three γ-proteobacteria *V. cholerae*, *S. enterica* and *E. coli* as well as the thin β-proteobacterium *Hylemonella gracilis* have similar cross-sections and diameters of ∼40 nm. The C-rings from *H. neptunium* and *C. crescentus* (both α-proteobacteria) are less clear (suggesting incomplete occupancy or mobility) and exhibit a distinctive conical reduction in diameters from, for example in *C. crescentus*, 36 nm near the inner membrane to 26 nm at the tip near the FliHIJ complex. The average diameter of the C-rings in the pathogenic ε-proteobacteria *C. jejuni* and *H. hepaticus* is 49 nm, and these display stronger densities at the membrane-proximal side of the C-ring next to the export platform immediately beneath the MS-ring. It is known that the membrane-proximal part of the C-ring is composed of FliG (Thomas *et al*, 2006; Liu *et al*, 2009); and therefore, these stronger densities may represent alternative, more stable, or higher occupancy conformations of FliG, or additional components of the motor exclusive to

the ε-proteobacteria. The spirochaetes *B. burgdorferi* and *T. primitia* and the diderm firmicute *A. longum* possess C-rings with an even larger average diameter of 54 nm, but maintain the same cross-section as *S. enterica*. No correlation could be made between tomographic density and the presence of FliY, a FliN paralogue with an additional domain found in *A. longum*, *T. primitia, H. hepaticus, C. jejuni* and *S. enterica*.

Rod and L/P-rings

Assembling atop the S-ring is the rod, which acts as the central driveshaft through the cell envelope, transmitting torque applied to the MS-ring to the hook and filament. The rod is comprised of ubiquitous paralogous proteins that are known to form a proximal (FliE, FlgB, FlgC and FlgF) and a distal (FlgG) rod, but no new details about the arrangement of these proteins could be gleaned from the tomograms. The length of the rod was well conserved, as judged by the distinct densities seen in the generic average for the S- and P-rings and inner and outer membranes. The distance between the distal end of the S-ring and the centre of the outer membrane was 22 nm (measured in the generic average), confirming earlier measurements of the rod length on isolated flagellar hook-basal bodies (HBBs) from wild-type *S. enterica* (Takahashi *et al*, 2009).

The periplasmic P- and L-rings around the rod are thought to function as bushings through the peptidoglycan layer and lipopolysaccharide of the outer membrane, respectively. Because the rings coat the outside of the rod, both proteins (FlgH and FlgI) are exported into the periplasm via the Sec pathway instead of through the dedicated flagellar T3SS (Homma *et al*, 1987; Jones and Macnab, 1990). Unlike the rod proteins, however, it has previously been noted that the genes encoding the L/P-ring components are not ubiquitous, and the variation seen here calls into question the presumed roles of these proteins (Pallen *et al*, 2005). The reconstructions of *S. enterica*, *E. coli*, *H. neptunium*, *C. crescentus* and *A. longum* represent the 'standard' cases, where both the L- and P-ring genes are present, the P-ring is visible in the tomograms, and the L-ring is not, likely because it is embedded in the outer membrane. In *H. gracilis*, both genes are present, and two rings are visible underneath the outer membrane, suggesting that the L-ring may not be embedded in the membrane in this species, although it is not clear why this alternative arrangement is seen. In the sheathed flagella of *H. hepaticus* and *V. cholerae,* the outer membrane continues as a sheath around the flagellar hook and filament. The L-ring proteins in these two organisms presumably still form a complex with the P-ring, but the diverse structures in that region make assignments unclear. It is noteworthy that the *H. hepaticus* L-ring gene does not encode an otherwise ubiquitous cysteine residue in the vicinity of the amino terminus (Schoenhals and Macnab, 1996). This residue has been shown to be part of a signal peptide II cleavage consensus motif that is subsequently lipoylated. The situation is further complicated by the fact that this cysteine residue is nevertheless retained in the other organism with a sheathed flagellum, *V. cholerae*. In the spirochaetes *B. burgdorferi* and *T. primitia*, the L-ring protein FlgH is absent, as is thought due to the fact that the flagellar filaments in these organisms never cross the outer membrane (Pallen *et al*, 2005), but remain within the periplasm. The P-ring protein FlgI is absent only in

the genome of *T. primitia*. This was first observed by tomography in a recent study of a *B. burgforferi* FlgI mutant, in which a density around the rod was absent (Liu *et al*, 2009). Here, we observe a similar absence of ring density on the rod of *T. primitia,* corresponding to FlgI. It is noteworthy that FlgI in the spirochaetes is distant from the peptidoglycan layer, at odds with its supposed function. FlgI is also found in the Leptospiraceae, another family within the spirochaete class, so it may have a special alternative function in the spirochaetes (Chevance *et al*, 2007).

Stator complex

Above the C-ring and surrounding the MS-ring in the inner membrane are stator complexes that are thought to extend towards and bind to the peptidoglycan layer. Through interactions with the C-ring proteins, the stators transform the flow of H^+ or Na^+ ions across the membrane into torque to drive the motor. Each stator complex is composed of two proteins, MotA and MotB in the H^+-dependent stators (e.g., *E. coli*), or PomA and PomB in the Na^+-dependent stators (e.g., *V. cholerae*), with an apparent 4:2 stoichiometry. In our averaged structures, we see distinctive rod-shaped stator ring structures above the inner membrane with connections on the other side of the membrane to the C-ring in the β-proteobacterium *H. gracilis* and the spirochaetes *B. burgdorferi* and *T. primitia*. As previously shown elsewhere (Murphy *et al*, 2006; Liu *et al*, 2009; Kudryashev *et al*, 2010) and reproduced in Figure 5, 16 copies of the stator complexes are clearly seen in the averaged tomograms of the spirochaetes *B. burgdorferi* and *T. primitia* even before rotational averaging. In contrast, the symmetry observed in the *H. gracilis* stator ring is 13 (Figure 5). In the α-proteobacteria (*H. neptunium* and *C. crescentus*), stator densities are visible, but they are less prominent and their symmetries could not be discerned. In the ε-proteobacteria *C. jejuni* and *H. hepaticus*, stator densities are clear, but they have a different shape in cross-section, lie nearly parallel to the cytoplasmic membrane, and extend further into the periplasm. The reason that the symmetry of these motors could not be discerned may be that the stator system is highly dynamic with rapid turnover of subunits (Leake *et al*, 2006) and perhaps variable conformations, causing low occupancy and heterogeneity. These cells also have single, polar flagella, and so because the rod-shaped cells freeze lying flat on the grid, no direct 'top' views of the motor were obtained, which makes detecting rotational symmetries more difficult. The rest of the species may not exhibit clear stator density because the periplasmic domains of the stator complex (MotA/B or PomA/B) are thin, as shown in cryoEM images of purified PomA/B in liposomes (Yonekura *et al*, 2006).

Unconserved densities

In addition to this somewhat conserved structural core, many of the organisms exhibited additional, presumably proteinaceous densities that are likely to be unrecognized, novel components of the motor. The most striking is the spirochaetes' large 'P-collar' that forms a bowl-like structure around the rod within the stator ring, and which has been postulated to stabilize the motor (Murphy *et al*, 2006). To generate hypotheses about which proteins form the P-collar, we exploited the fact that genes encoding proteins involved in stable complexes are frequently encoded in genomic proximity
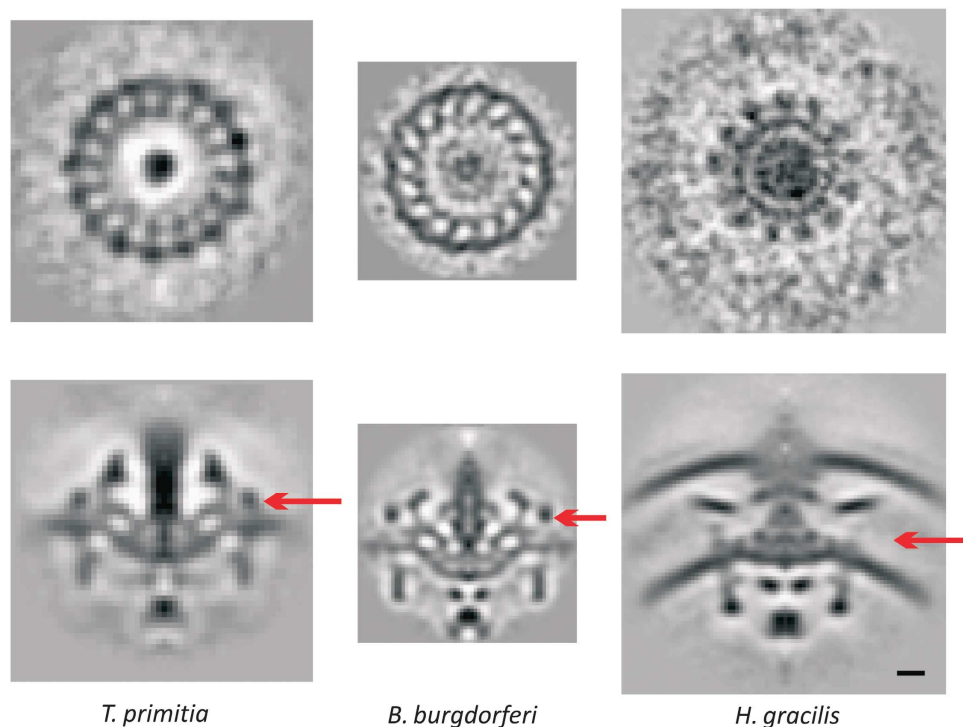
Figure 5 Symmetries in the stator region. Upper row: Radial slices through the stator regions of three average motors before rotational averaging showing 16-, 16- and 13-fold symmetry, respectively. Lower row: Axial slices through the averaged and symmetrized motors with arrows showing the height at which the radial slices were taken. Scale bar, 10 nm.

to one-another (Huynen *et al*, 2000). Furthermore, as the protein is not a component of the cylindrical core of the rod, hook or filament, we assumed its secretion would be via the Sec pathway as opposed to the dedicated flagellar T3SS. Using these criteria (see Materials and methods), we narrowed our search to a candidate gene for involvement in the P-collar, flbB, first identified in a comprehensive study of *B. burgdorferi* flagellar genetics (Ge *et al*, 1997). This gene is consistently near other flagellar motor genes in spirochaetes and includes the appropriate periplasmic export signal.

While the L/P-ring complex simply surrounds the rod as it passes through the lipopolysaccharide membrane and peptidoglycan layer in the well-studied flagellar motors, in *V. cholerae* it appears to serve as a foundation for two additional structures. *V. cholerae* possesses two proteins, MotX and MotY, which form a so-called T-ring that is thought to assist in the formation and binding of the MotA/MotB stators (Terashima *et al*, 2006). Here, this T-ring can be seen lower and to the outside of the P-ring, to which it is connected. There is also a substantial increase in density near the presumed position of the L-ring. Hosogi *et al* (2011) recently described this entire density in the closely related *Vibrio alginolyticus* HBB as the L-ring. Based on the fact that the L-ring-encoding *flgH* gene is ∼360 amino acids long in both *S. enterica* and *V. cholerae*, we propose that the unusually large and oddly shaped ring structure must also include an additional, as-yet unidentified protein.

The L/P-ring complex also appears to serve as a structural anchor in the ε-proteobacteria *C. jejuni* and *H. hepaticus*. Here, the L/P-ring complex is attached to large periplasmic basal disks. In *C. jejuni*, an extensive disk-like density is

found in the periplasm immediately below and parallel to the outer membrane around the rod and above the stators. This disk connects to the P-ring and has an outer radius of 48 ± 9 nm, calculated from the edge of the rod along the disk. A second disk with a radius of 32 ± 7 nm sits beneath the first and seems to be faintly connected to the M/S-ring. In *H. hepaticus*, a similarly extensive (32 ± 2 nm in radius) but flat disk is found between what are probably enhanced L- and P-rings. A similarly large disk (85 nm average radius) connected to the L/P-ring complex was observed previously by EM of negatively stained flagellar motors purified from another ε-proteobacterium, *Wolinella succinogenes*, which is closely related to *C. jejuni* and *H. hepaticus* (Engelhardt *et al*, 1993). While all three of these large basal disks are likely composed of homologous proteins, bioinformatic analyses yielded no candidate proteins for this structure, likely unaided by the well-discussed genomic fragmentation and lack of synteny within the ε-proteobacteria (Eppinger *et al*, 2004).

It is interesting to note that the β-proteobacterium *H. gracilis* also exhibited a periplasmic disk above the stators, but the relationship of this disk to the larger ε-proteobacterial basal disks is unclear. The *H. gracilis* disk is at the same height as the P-ring but does not connect, exhibiting an inner and outer radius of 18 ± 2 and 31 ± 2 nm, respectively. Previously, similar disks have been observed in another β-proteobacterium, *Aquaspirillum serpens* (Coulton and Murray, 1978). The function of these disks remains unclear, as their occurrence does not seem to correlate with any obvious phenotype (such as sheathed flagella) or habitat (such as viscous environment), besides that they are so far exclusive to (but not

required for) polar flagella. Based on their position, they may stabilize the stators to sustain larger torques.

Above the basal disk and immediately below the highly curved bend in the outer membrane of the sheathed *H. hepaticus* is yet another disk-like density. As mentioned above, in the other sheathed bacterium, *V. cholerae*, the L-ring is unusually large and odd-shaped. These structures may stabilize the outer membrane and the sheath against the rotation of the flagellum. Finally, two previous studies of negatively stained, purified *C. crescentus* motors gave conflicting reports about whether or not a so-called E-ring existed between the M/S- and L/P-ring complexes (Stallmeyer *et al*, 1989; Kanbe *et al*, 2005). It remains unclear whether there are additional rings here in the *C. crescentus* and *H. neptunium* reconstructions.

Conclusion

In summary, three-dimensional structures of 11 phylogenetically diverse bacterial flagellar motors were obtained *in situ* at a few nanometre resolutions via ECT and subtomogram averaging. The positions of key proteins of the export apparatus were determined. While the motors all exhibited a common core built from the products of conserved flagellar genes, their overall appearances were strikingly different due to variations in the structure of that core and the presence of unique peripheral densities, showing that each is a related but specially adapted nanomachine.

Materials and methods

Culture conditions

C. crescentus CB15N, *E. coli* RP437 and MG1655, *V. cholerae* TRH7000, *H. hepaticus* (ATCC 51449), *C. jejuni* (ATCC 29428), *B. burgdorferi* B31 (ATCC 35210), *A. longum* APO-1 DSM 6540 and *T. primitia* strain ZAS-2 cells were grown as described previously (Murphy *et al*, 2006; Briegel *et al*, 2009).

H. neptunium (ATCC 15444) was grown in 2216 marine broth (Difco) at 30°C for 24–48 h. The cell culture was incubated on ice during plunge freezing.

S. enterica subsp. enterica serovar Typhimurium str. LT2 was grown in LB plus 0.3 M sucrose and up to 10 mM MgSO$_4$. Penicillin (466 IU/ml) was added 15 and 60 min before plunge freezing.

H. gracilis was cultivated from a rotten lily taken from a Caltech pond by placing a drop of liquid upon a 0.22-μm filter resting atop agar containing 10 mM MOPS pH 7.0, 0.5 g tryptone and 0.5 g yeast extract per litre. Colonies appeared several weeks later. The 16S rRNA was sequenced from a liquid culture and found to be identical to the type strain of *H. gracilis*. Cultures were grown in the above media without MOPS for 2 days and only reached an OD of 0.05. The cells were checked for motility with a light microscope. The cells were then centrifuged and concentrated 10-fold in the same media for plunge freezing onto the EM grids (Murphy, 2007).

Genome sequencing

H. gracilis (ATCC 19624) cultures were obtained from the ATCC and cultured in liquid and agar media containing 5 g peptone, 0.5 g yeast extract, 0.02 g Tween-80 and 0.1 g K$_2$HPO$_4$ made up to 1 l with nanopure water with optional addition of 15 g agar. Colonies were initially grown on agar plates and subsequently used to inoculate liquid cultures. The identity of the cultures was confirmed by PCR amplification and sequencing of 16S rRNA. DNA was purified from 2 l cultures by lysing cells with lysozyme followed by consecutive RnaseA, proteinase K, SDS, sodium acetate and chloroform/phenol mixture additions. DNA was washed with ethanol and dried. A paired-end genomic DNA library was prepared from this sample and 76 bp reads generated using Illumina sequencing at Caltech's Millard & Muriel Jacobs Genetics & Genomics Laboratory (http://mmjggl.caltech.edu/sequencing/). Reads were truncated to 67 bp and assembled using Velvet (Zerbino and Birney, 2008). Using a

kmer size of 49, 3.6 Mb of sequence data was generated and distributed over 152 contigs with an n_{50} of 75 kb and a maximum contig length of 192 kb. This partially assembled genome was annotated for ORFs using the NCBI PGAAP service and flagellar genes semi-automatically annotated using reciprocal best-hit methodology and manual curation. This Whole Genome Shotgun project has been deposited at DDBJ/EMBL/GenBank under the accession AEGR00000000. The version described in this paper is the first version, AEGR01000000.

The genome sequencing of *A. longum* APO-1 was performed at Stanford in the laboratory facility of Stephen Quake and will be described elsewhere. This Whole Genome Shotgun project has been deposited at DDBJ/EMBL/GenBank under the accession AFGF00000000. The version described in this paper is the first version, AFGF01000000. Genome sequencing results for *T. primitia* ZAS-2 will be described elsewhere; the closed sequence for this strain has been deposited into GenBank as CP001843.

EM sample preparation, data collection and tomogram reconstruction

EM R2/2 copper/rhodium Quantifoil or lacy carbon grids were glow discharged and coated with a 3 × -concentrated solution of 10 nm colloidal gold particles (Ted Pella). A 5 × -concentrated solution of 10 nm colloidal gold was also added to the cells immediately before plunge freezing. A 4-μl droplet of the sample solution was applied to the EM grid, then blotted and plunge frozen into liquid ethane (Dubochet *et al*, 1988) or into a liquid ethane–propane mixture (Tivol *et al*, 2008) using a Vitrobot (FEI Company) (Iancu *et al*, 2006) or in-house plunger. To flatten the thickest cell types, *E. coli* and *S. enterica* cells were incubated with 466 IU/ml penicillin G for up to 60 min at 30°C (Eisenbach and Adler, 1981), which caused some cells to rupture when blotted just before plunge freezing. The grids were stored under liquid nitrogen until data collection.

EM images were collected using a Polara 300-kV FEG transmission electron microscope (FEI Company) equipped with an energy filter (slit width 20 eV; Gatan) on a 2k × 2k Ultrascan CCD camera or, later, a lens-coupled 4k × 4k UltraCam (Gatan). Typically, tilt series were recorded from −60° to 60° with an increment of 1° semi-automatically around 1 or 2 axes (Iancu *et al*, 2005) at 8–12 μm under-focus using the predictive UCSF-Tomo package (Zheng *et al*, 2007) or Leginon (Suloway *et al*, 2009). Cumulative doses of up to 200 e$^-$/Å^2 were used.

Image tilt series were generally binned by two (in X and Y) and 3D tomograms were calculated automatically by Raptor (Amat *et al*, 2008) using the Peach distributed computing system (Leong *et al*, 2005). In cases where Raptor was not available or failed, the semi-automatic IMOD software package (Mastronarde, 1997) was used. No digital filters were used to reduce noise. Image tilt series and final reconstructions were deposited into an in-house web-based database. For a more detailed protocol, see Chen *et al* (2010).

Subtomogram extraction, alignment, averaging and symmetrization

Bsoft (Heymann *et al*, 2008) and the Peach (Leong *et al*, 2005) distributed computing system were used for iterative subtomogram extraction, alignment, averaging and symmetrization. For *V. cholerae*, *H. neptunium* and *A. longum*, tomograms of different magnifications were used, and the tomograms of higher magnification were re-sampled to match the pixel size of the tomograms of lowest magnification. The positions of flagellar motors in the tomograms were marked by eye at the entry point of the flagellar filament into the outer membrane. For alignment, subtomograms centred on the motors were extracted, bandpass filtered between 200 nm and the first CTF zero and masked in reciprocal space within the missing wedge. Rotational alignments were done with 3° step sizes, as no further improvement was seen with finer steps. Subtomograms containing flagellar motors were first extracted by hand and aligned to a reference arbitrarily chosen from the data sets. The aligned motors were then averaged, and the average was rotated so that the rod axis coincided with the z-axis. This result was cylindrically symmetrized around the z-axis. Subtomograms were computationally re-extracted based on the previous alignment result, realigned to the symmetrized average motor, re-averaged and symmetrized. The whole process was iterated until the coordinates of motors stabilized. Average motors were checked computationally for symmetry about the rod before applying any symmetry. In the cases of the spirochaetes and *H. gracilis*, where

symmetry was detected in the stator rings, the average reconstruction was symmetrized accordingly (16- and 13-fold, respectively). In all other cases, 16-fold symmetry was applied simply to improve the signal-to-noise ratio of the final motor structure. Note the cylindrical symmetrization does not affect the axial structures obtained as shown in Figure 1. All the symmetrized average motor structures have been deposited into the EMDataBank.

Tomograms were inspected and measured with IMOD (Mastronarde, 1997). 2D image thresholding and superposition was done with Adobe Photoshop (Adobe Systems Inc.). The resolution was estimated by separately averaging and symmetrizing two halves of the data set and correlating them using Fourier shell correlation with a threshold of 0.5 (Supplementary Figure S1).

Identification of FliI location
Starting with wild-type *Campylobacter jejuni* 81-176 Sm^R (DRH212) containing an *rpsL* allele conferring streptomycin resistance (Hendrixson *et al*, 2001), strain DRH2257 was constructed through in-frame deletions of *fliI* and marker gene *astA* (the enzyme arylsulphatase), which does not affect flagellar biosynthesis or motility (Joslin and Hendrixson, 2009). DRH212 and DRH2257 were grown on MH agar under microaerophilic conditions for 3 days, re-streaked and grown overnight. Colonies were resuspended in MH broth, plunge frozen and imaged as described above except that images were collected at $-15 \mu m$ defocus. Subtomographic averages were generated from 21 wild-type and 19 $\Delta fliI$ motors, respectively, using PEET from the IMOD suite of programs without symmetrization (Mastronarde, 1997).

Bioinformatics analysis
To define orthologous gene families, flagellar structural protein genes were initially grouped according to the KEGG Orthology (KO) Database (Kanehisa *et al*, 2010). Family assignments were verified and/or revised by extensive literature searches and manual BLASTing to confirm the automated KO assignments. For those genomes not covered by the KO Database, genes were assigned to orthologous gene families by BLAST reciprocal best-hit methods against the previously curated family allocations. Non-flagellar gene family assignments were made automatically using the KO Database without further manual curation.

To predict functional linkages between known flagellar genes and novel genes, the mutual information score was calculated between operon occurrence vectors of each orthologous gene family using a previously described operon prediction method (Overbeek *et al*, 1999). An operon occurrence vector describes in which operons a given orthologous gene family resides: that is, for each orthologous family, a binary vector is assigned of dimension equal to the number of operons in the combined sequenced genomes used for this analysis. Thus, each gene family's operon occurrence vector will be predominantly '0', with occasionally a '1' for those operons in which that family occurs. For each defined novel substructure observed by tomography (e.g., the P-collar), the subset of organisms in which it is found were noted, and the mutual information between all gene families exclusive to that subset was calculated. Orthologous families predicted to be functionally linked to known flagellar genes by a high mutual information score were further filtered for periplasmic export sequences using SignalP (Emanuelsson *et al*, 2007).

Supplementary data
Supplementary data are available at *The EMBO Journal* Online (http://www.embojournal.org).

Conflict of interest

The authors declare that they have no conflict of interest.

References

Amat F, Moussavi F, Comolli LR, Elidan G, Downing KH, Horowitz M (2008) Markov random field based automatic image alignment for electron tomography. *J Struct Biol* **161:** 260–275

Berg HC (2003) The rotary motor of bacterial flagella. *Annu Rev Biochem* **72:** 19–54

Briegel A, Ortega DR, Tocheva EI, Wuichet K, Li Z, Chen SY, Muller A, Iancu CV, Murphy GE, Dobro MJ, Zhulin IB, Jensen GJ (2009) Universal architecture of bacterial chemoreceptor arrays. *Proc Natl Acad Sci USA* **106:** 17181–17186

Chen S, McDowall A, Dobro MJ, Briegel A, Ladinsky M, Shi J, Tocheva EI, Beeby M, Pilhofer M, Ding HJ, Li Z, Gan L, Morris DM, Jensen GJ (2010) Electron cryotomography of bacterial cells. *J Vis Exp* **39**; doi:10.3791/1943, http://www.jove.com/details.stp?id=1943

Chevance FFV, Hughes KT (2008) Coordinating assembly of a bacterial macromolecular machine. *Nat Rev Microbiol* **6:** 455–465

Chevance FFV, Takahashi N, Karlinsey JE, Gnerer J, Hirano T, Samudrala R, Aizawa SI, Hughes KT (2007) The mechanism of outer membrane penetration by the eubacterial flagellum and implications for spirochete evolution. *Genes Dev* **21:** 2326–2335

Claret L, Calder SR, Higgins D, Hughes C (2003) Oligomerization and activation of the FliI ATPase central to bacterial flagellum assembly. *Mol Microbiol* **48:** 1349–1355

Coulton JW, Murray RGE (1978) Cell envelope associations of Aquaspirillum Serpens flagella. *J Bacteriol* **136:** 1037–1049

Dubochet J, Adrian M, Chang JJ, Homo JC, Lepault J, McDowall AW, Schultz P (1988) Cryo-Electron Microscopy of vitrified specimens. *Q Rev Biophys* **21:** 129–228

Eisenbach M, Adler J (1981) Bacterial-cell envelopes with functional flagella. *J Biol Chem* **256:** 8807–8814

Emanuelsson O, Brunak S, von Heijne G, Nielsen H (2007) Locating proteins in the cell using TargetP, SignalP and related tools. *Nat Protoc* **2:** 953–971

Engelhardt H, Schuster SC, Baeuerlein E (1993) An archimedian spiral—the basal disk of the Wolinella Flagellar Motor. *Science* **262:** 1046–1048

Eppinger M, Baar C, Raddatz G, Huson DH, Schuster SC (2004) Comparative analysis of four Campylobacterales. *Nat Rev Microbiol* **2:** 872–885

Galkin VE, Yu X, Bielnicki J, Heuser J, Ewing CP, Guerry P, Egelman EH (2008) Divergence of quaternary structures among bacterial flagellar filaments. *Science* **320:** 382–385

Ge Y, Old IG, Saint Girons I, Charon NW (1997) Molecular characterization of a large Borrelia burgdorferi motility operon which is initiated by a consensus sigma70 promoter. *J Bacteriol* **179:** 2289–2299

Hazelbauer GL, Falke JJ, Parkinson JS (2008) Bacterial chemoreceptors: high-performance signaling in networked arrays. *Trends Biochem Sci* **33:** 9–19

Hendrixson DR, Akerley BJ, DiRita VJ (2001) Transposon mutagenesis of Campylobacter jejuni identifies a bipartite energy taxis system required for motility. *Mol Microbiol* **40:** 214–224

Heymann JB, Cardone G, Winkler DC, Steven AC (2008) Computational resources for cryo-electron tomography in Bsoft. *J Struct Biol* **161:** 232–242

Homma M, Komeda Y, Iino T, Macnab RM (1987) The flaFIX gene product of Salmonella typhimurium is a flagellar basal body component with a signal peptide for export. *J Bacteriol* **169:** 1493–1498

Hosogi N, Shigematsu H, Terashima H, Homma M, Nagayama K (2011) Zernike phase contrast cryo-electron tomography of sodium-driven flagellar hook-basal bodies from Vibrio alginolyticus. *J Struct Biol* **173:** 67–76

Huynen M, Snel B, Lathe W, Bork P (2000) Predicting protein function by genomic context: quantitative evaluation and qualitative inferences. *Genome Res* **10:** 1204–1210

Iancu CV, Tivol WF, Schooler JB, Dias DP, Henderson GP, Murphy GE, Wright ER, Li Z, Yu Z, Briegel A, Gan L, He Y, Jensen GJ (2006) Electron cryotomography sample preparation using the Vitrobot. *Nat Protoc* **1:** 2813–2819

Iancu CV, Wright ER, Benjamin J, Tivol WF, Dias DP, Murphy GE, Morrison RC, Heymann JB, Jensen GJ (2005) A 'flip-flop' rotation stage for routine dual-axis electron cryotomography. *J Struct Biol* **151:** 288–297

Ibuki T, Imada K, Minamino T, Kato T, Miyata T, Namba K (2011) Common architecture of the flagellar type III protein export apparatus and F- and V-type ATPases. *Nat Struct Mol Biol* **18:** 277–282

Imada K, Minamino T, Tahara A, Namba K (2007) Structural similarity between the flagellar type III ATPase FliI and F-1-ATPase subunits. *Proc Natl Acad Sci USA* **104:** 485–490

Jones CJ, Macnab RM (1990) Flagellar assembly in Salmonella typhimurium: analysis with temperature-sensitive mutants. *J Bacteriol* **172:** 1327–1339

Joslin SN, Hendrixson DR (2009) Activation of the Campylobacter jejuni FlgSR two-component system is linked to the flagellar export apparatus. *J Bacteriol* **191:** 2656–2667

Kanbe M, Shibata S, Umino Y, Jenal U, Aizawa SI (2005) Protease susceptibility of the Caulobacter crescentus flagellar hook-basal body: a possible mechanism of flagellar ejection during cell differentiation. *Microbiology* **151:** 433–438

Kanehisa M, Goto S, Furumichi M, Tanabe M, Hirakawa M (2010) KEGG for representation and analysis of molecular networks involving diseases and drugs. *Nucleic Acids Res* **38:** D355–D360

Katayama E, Shiraishi T, Oosawa K, Baba N, Aizawa S (1996) Geometry of the flagellar motor in the cytoplasmic membrane of Salmonella typhimurium as determined by stereo-photogrammetry of quick-freeze deep-etch replica images. *J Mol Biol* **255:** 458–475

Kudryashev M, Cyrklaff M, Wallich R, Baumeister W, Frischknecht F (2010) Distinct *in situ* structures of the Borrelia flagellar motor. *J Struct Biol* **169:** 54–61

Leake MC, Chandler JH, Wadhams GH, Bai F, Berry RM, Armitage JP (2006) Stoichiometry and turnover in single, functioning membrane protein complexes. *Nature* **443:** 355–358

Leong PA, Heymann JB, Jensen GJ (2005) Peach: a simple Perl-based system for distributed computation and its application to cryo-EM data processing—Ways & means. *Structure* **13:** 505–511

Li Z, Jensen GJ (2009) Electron cryotomography: a new view into microbial ultrastructure. *Curr Opin Microbiol* **12:** 333–340

Liu J, Lin T, Botkin DJ, McCrum E, Winkler H, Norris SJ (2009) Intact flagellar motor of Borrelia burgdorferi revealed by cryo-electron tomography: evidence for stator ring curvature and rotor/C-ring assembly flexion. *J Bacteriol* **191:** 5026–5036

Liu RY, Ochman H (2007) Stepwise formation of the bacterial flagellar system. *Proc Natl Acad Sci USA* **104:** 7116–7121

Mastronarde DN (1997) Dual-axis tomography: an approach with alignment methods that preserve resolution. *J Struct Biol* **120:** 343–352

McCarter LL (2004) Dual flagellar systems enable motility under different circumstances. *J Mol Microbiol Biotechnol* **7:** 18–29

McCarter LL (2006) Regulation of flagella. *Curr Opin Microbiol* **9:** 180–186

Milne JLS, Subramaniam S (2009) Cryo-electron tomography of bacteria: progress, challenges and future prospects. *Nat Rev Microbiol* **7:** 666–675

Minamino T, Imada K, Namba K (2008) Molecular motors of the bacterial flagella. *Curr Opin Struct Biol* **18:** 693–701

Miwa K, Yoshida M (1989) The alpha 3 beta 3 complex, the catalytic core of F1-ATPase. *Proc Natl Acad Sci USA* **86:** 6484–6487

Moore SA, Jia YH (2010) Structure of the cytoplasmic domain of the flagellar secretion apparatus component FlhA from Helicobacter pylori. *J Biol Chem* **285:** 21060–21069

Murphy GE (2007) *Cryoelectron Tomography of Bacteria and Their Macromolecular Machines*. Pasadena, USA: California Institute of Technology

Murphy GE, Leadbetter JR, Jensen GJ (2006) *In situ* structure of the complete Treponema primitia flagellar motor. *Nature* **442:** 1062–1064

Overbeek R, Fonstein M, D'Souza M, Pusch GD, Maltsev N (1999) The use of gene clusters to infer functional coupling. *Proc Natl Acad Sci USA* **96:** 2896–2901

Pallen MJ, Matzke NJ (2006) From the origin of species to the origin of bacterial flagella. *Nat Rev Microbiol* **4:** 784–790

Pallen MJ, Penn CW, Chaudhuri RR (2005) Bacterial flagellar diversity in the post-genomic era. *Trends Microbiol* **13:** 143–149

Paul K, Erhardt M, Hirano T, Blair DF, Hughes KT (2008) Energy source of flagellar type III secretion. *Nature* **451:** 489–492

Saijo-Hamano Y, Imada K, Minamino T, Kihara M, Shimada M, Kitao A, Namba K (2010) Structure of the cytoplasmic domain of FlhA and implication for flagellar type III protein export. *Mol Microbiol* **76:** 260–268

Saijo-Hamano Y, Minamino T, Macnab RM, Namba K (2004) Structural and functional analysis of the C-terminal cytoplasmic domain of FlhA, an integral membrane component of the type III flagellar protein export apparatus in Salmonella. *J Mol Biol* **343:** 457–466

Schoenhals GJ, Macnab RM (1996) Physiological and biochemical analyses of FlgH, a lipoprotein forming the outer membrane L ring of the flagellar basal body of Salmonella typhimurium. *J Bacteriol* **178:** 4200–4207

Snyder LAS, Lornan NJ, Futterer K, Pallen MJ (2009) Bacterial flagellar diversity and evolution: seek simplicity and distrust it? *Trends Microbiol* **17:** 1–5

Sowa Y, Berry RM (2008) Bacterial flagellar motor. *Q Rev Biophys* **41:** 103–132

Stallmeyer MJB, Hahnenberger KM, Sosinsky GE, Shapiro L, Derosier DJ (1989) Image reconstruction of the flagellar basal body of Caulobacter crescentus. *J Mol Biol* **205:** 511–518

Suloway C, Shi J, Cheng A, Pulokas J, Carragher B, Potter CS, Zheng SQ, Agard DA, Jensen GJ (2009) Fully automated, sequential tilt-series acquisition with Leginon. *J Struct Biol* **167:** 11–18

Suzuki H, Yonekura K, Namba K (2004) Structure of the rotor of the bacterial flagellar motor revealed by electron cryomicroscopy and single-particle image analysis. *J Mol Biol* **337:** 105–113

Takahashi N, Mizuno S, Hirano T, Chevance FFV, Hughes KT, Aizawa SI (2009) Autonomous and FliK-dependent length control of the flagellar rod in Salmonella enterica. *J Bacteriol* **191:** 6469–6472

Terashima H, Fukuoka H, Yakushi T, Kojima S, Homma M (2006) The Vibrio motor proteins, MotX and MotY, are associated with the basal body of Na + -driven flagella and required for stator formation. *Mol Microbiol* **62:** 1170–1180

Thomas DR, Francis NR, Xu C, DeRosier DJ (2006) The three-dimensional structure of the flagellar rotor from a clockwise-locked mutant of Salmonella enterica serovar Typhimurium. *J Bacteriol* **188:** 7039–7048

Tivol WF, Briegel A, Jensen GJ (2008) An improved cryogen for plunge freezing. *Microsc Microanal* **14:** 375–379

Worrall LJ, Vuckovic M, Strynadka NCJ (2010) Crystal structure of the C-terminal domain of the Salmonella type III secretion system export apparatus protein InvA. *Protein Sci* **19:** 1091–1096

Yonekura K, Yakushi T, Atsumi T, Maki-Yonekura S, Homma M, Namba K (2006) Electron cryomicroscopic visualization of PomA/B stator units of the sodium-driven flagellar motor in liposomes. *J Mol Biol* **357:** 73–81

Zarivach R, Deng WY, Vuckovic M, Felise HB, Nguyen HV, Miller SI, Finlay BB, Strynadka NCJ (2008) Structural analysis of the essential self-cleaving type III secretion proteins EscU and SpaS. *Nature* **453:** 124–127

Zarivach R, Vuckovic M, Deng WY, Finlay BB, Strynadka NCJ (2007) Structural analysis of a prototypical ATPase from the type III secretion system. *Nat Struct Mol Biol* **14:** 131–137

Zerbino DR, Birney E (2008) Velvet: algorithms for *de novo* short read assembly using de Bruijn graphs. *Genome Res* **18:** 821–829

Zheng SQ, Keszthelyi B, Branlund E, Lyle JM, Braunfeld MB, Sedat JW, Agard DA (2007) UCSF tomography: an integrated software suite for real-time electron microscopic tomographic data collection, alignment, and reconstruction. *J Struct Biol* **157:** 138–147